Oxygen Reduction on Iron−Melanin Granular Surfaces

Alejandro González Orive,[§] Alberto Hernández Creus,[§] Doris Grumelli,[†] Guillermo A. Benitez,[†] Leandro Andrini,[‡] Felix G. Requejo,[‡] Cecilia Bonazzola,[||] and Roberto C. Salvarezza*[,†]

Instituto de Investigaciones Fisicoquímicas, Teóricas y Aplicadas, CONICET-Universidad Nacional de La Plata, Sucursal 4 Casilla de Correo 16, La Plata 1900, Argentina, Instituto de Investigaciones Fisicoquímicas, Teóricas y Aplicadas and Departamento de Física, CONICET-Universidad Nacional de La Plata, Argentina, Departamento de Química Física, Universidad de la Laguna, La Laguna, Tenerife, Spain, and Departamento de Química Inorgánica, Analítica y Química Física, Facultad de Ciencias Exactas y Naturales, Universidad de Buenos Aires, Argentina

Received: June 14, 2009; Revised Manuscript Received: August 13, 2009

We report the catalytic activity of iron−eumelanin granular deposits supported on graphite for the oxygen reduction in neutral and alkaline solutions. These deposits contain quinone groups and iron−melanin complexes as revealed by XPS, XANES, EXAFS, and IR spectroscopy. Voltammetric data show that the iron−eumelanin system exhibits higher electrocatalytic activity than quinone/hydroquinone films (Q/QH) on the same substrate. In contrast to Q/QH deposits, the iron-containing eumelanin system is able to reduce oxygen with transfer of four electrons, thus allowing the formation of reactive hydroxyl species. Our results can explain the physical chemistry basis of the oxygen-radical induced lipid peroxidation and consequent neurodegeneration of the melanin-containing dopaminergic neurons observed by several authors.

Introduction

Melanins are one class of biopolymers that have interesting physical and chemical properties such as photoactivity, electrochemical response, amorphous semiconductor behavior,[1] and high affinity for complexing metallic cations such as Fe, Cu, Zn, etc.[2] In normal circumstances melanins participate in scavenging free radicals probably by hydroxyl degradation of the biopolymer.[3] However, in certain conditions when large amounts of Fe(III) are available it is proposed that melanin enhances the formation of oxygen reactive species able to produce lipid peroxidation.[3−5] Therefore, iron−melanin could become the source of free radicals and cytotoxic compounds upon degradation of highly pigmented neurons, thereby perpetuating a cycle of oxidative stress and neuronal loss.[4] However, the understanding of the physical chemistry of these processes is difficult because the melanin structure is not completely known and it contains proteins, lipids, and metallic cations.

Recently we have shown that ultrathin films of eumelanins can be formed by electrochemical-induced deposition on Au(111)[6] and highly oriented pyrolityc graphite (HOPG)[7] from alkaline solutions containing synthetic eumelanin. In this case, the film exhibits the hierarchical structure found in natural melanin with melanin aggregates with sizes ranging from 5 to 50 nm.[6,7] We have also shown that the melanin films on Au[6] and HOPG[7] contain a small amount of Fe(II)/Fe(III) species and also that the films exhibit catalytic activity for hydrogen peroxide electroreduction, similar to those found for Fe-containing porphyrins.[8] In principle, the iron−melanin film can be used as biomimetic system to study the oxygen reduction on melanin granules in a controlled way by using electrochemical tools.

In this work we report the electrocatalytic activity of iron−melanin granular deposits supported on HOPG for the oxygen electroreduction and compare it with that found for quinone/hydroquinone (Q/HQ) deposits on the same substrate. Quinone and the semiquinone free radical intermediates are moieties in most human melanin structures.[9] Physisorbed or chemisorbed monolayers of several quinones, including duroquinone, anthraquinone, and dopamine itself, are catalytic toward different electrochemical reactions.[10] It has also been reported that dopamine-containing solutions allow the production of thin melanin-like films on a variety of different solids substrates by dip-coating.[11,12]

We have found that the oxygen electroreduction is catalyzed by iron−melanin deposits on HOPG. In contrast to the Q/HQ deposits on the same substrate, the iron−melanin system allows the complete reduction of oxygen to hydroxyl ions with exchange of four electrons. The first step, the reduction from oxygen to hydrogen peroxide, involves the Q/HQ redox couple while the second step from hydrogen peroxide to hydroxyl ions involves the Q/HQ/iron system.

Experimental Section

Melanin deposits were electrochemically prepared as described in ref 7. The HOPG substrates were immersed in a synthetic eumelanin-containing aqueous 0.1 M NaOH solution (0.3 g L^{-1}, melanin from Sigma, M8631). This solution also contains ∼0.3 ppm of Fe, as determined by atomic absorption spectroscopy.[6] The HOPG substrate was polarized at −1.0 V in a conventional three-electrode electrochemical cell containing the melanin solution for different times (4 h < t < 8 h) in order to coat the HOPG with the melanin-Fe deposit. Q/HQ deposits were prepared by using the same electrochemical procedure from

* To whom correspondence should be addressed. E-mail: robsalva@inifta.unlp.edu.ar. Fax: 542214254642. Phone: 54221425430. Website: http//nano.quimica.unlp.edu.ar.

[†] Instituto de Investigaciones Fisicoquímicas, Teóricas y Aplicadas, CONICET-Universidad Nacional de La Plata.

[‡] Instituto de Investigaciones Fisicoquímicas, Teóricas y Aplicadas and Departamento de Física, CONICET-Universidad Nacional de La Plata.

[§] Universidad de la Laguna.

[||] Universidad de Buenos Aires.

10.1021/jp905560d CCC: $40.75
Published on Web 09/03/2009

an alkaline solution containing the result of the oxidative polymerization of hydroquinone (Sigma H9003).[13] The charge density involved during the formation of the Q/HQ deposit on the HOPG surface was ≈0.3 C cm^{-2}, a figure equivalent to that obtained for $t = 8$ h of synthetic eumelanin deposition.

The oxygen electroreduction reaction was studied in oxygen containing TRIS (tris(hydroximethyl)aminomethane)HCl buffer) at pH 7.4 and 0.1 M NaOH solutions at room temperature and without stirring of the solutions. In all electrochemical measurements a saturated calomel electrode (SCE) and a platinum foil were used as reference and counterelectrode, respectively. Characterization of the Fe−melanin deposits on the HOPG surface was made using atomic force microscopy (AFM) and magnetic force microscopy (MFM) (Nanoscope IIIa, Veeco Instruments). MFM images were performed by interleaving the topographic scan with the "Lift mode" scan, i.e., the AFM tip was made to scan the sample at lift heights ranging from 25 to 50 nm above the topographic height of the sample at each point in order to prevent any topographic effect. Images were taken at a scanning rate of 1 Hz with tips coated with magnetic CoCr film working at a drive frequency of ca. 65 kHz. X-ray phothoelectron spectroscopy (XPS) was made using a Mg Kα source, XR50 (Specs GmbH), and a hemispherical electron energy analyzer (PHOIBOS 100, Specs GmbH).

Different oxygen concentrations were used. The highest concentration was prepared by oxygen bubbling into the different solutions for 5 min. Solutions containing lower levels of oxygen were prepared starting from the oxygen-saturated solution by nitrogen bubbling for different times. Immediately afterward, the diffusional limiting current corresponding to the oxygen electroreduction on a smooth platinum electrode with real surface area of 1 cm^2 was recorded in each solution. Then, the oxygen concentration was calculated from the Cottrell equation by using the measured diffusional currents and taking the saturated oxygen concentration at 25 °C equal to 1.2×10^{-3} M as it has been reported for pH values ranging from 5.5 to 13.[14a,b]

FTIR studies were carried out with a Bruker IFS66/ Spectrometer provided with a Globar detector and a crystal diamond ATR module. For each spectrum 128 interferograms were collected with a resolution of 8 cm^{-1}. Spectra are represented as the ratio R/R_0 where R and R_0 are the reflectance corresponding to the sample and to the HOPG free surface, respectively.

X-ray absorption near-edge structure spectroscopy (XANES) and extended X-ray absorption fine structure (EXAFS) were employed to analyze the nature of the synthetic eumelanin solid sample. The X-ray absorption spectra were measured at the XAFS-1 beamline of the LNLS, Laboratorio Nacional do Luz Síncrotron, Campinas, São Paulo, Brazil. XANES and EXAFS spectra at the Fe K-edge (7112 eV) were recorded in air at room temperature in transmission mode with three ion chambers as detectors: one before the sample to measure the incident X-ray intensity (I_0), one after the sample and before the corresponding reference metal foil to measure the intensity after the sample (I_1), and one after the metal foil (I_2). The absorption spectrum of the sample and the metal foil were expressed as $\log(I_0/I_1)$ and $\log(I_1/I_2)$, respectively. The spectrum of the metal foil was used to calibrate the absolute energy scale for the corresponding sample spectrum by positioning the absorption edge at the first inflection point. Monochromator at the beamline was equipped with Si(111) crystals. The 0.3 mm vertical aperture of the beam definition slits in the hutch provided a resolution of about 2.5 eV at the Fe K-edge.

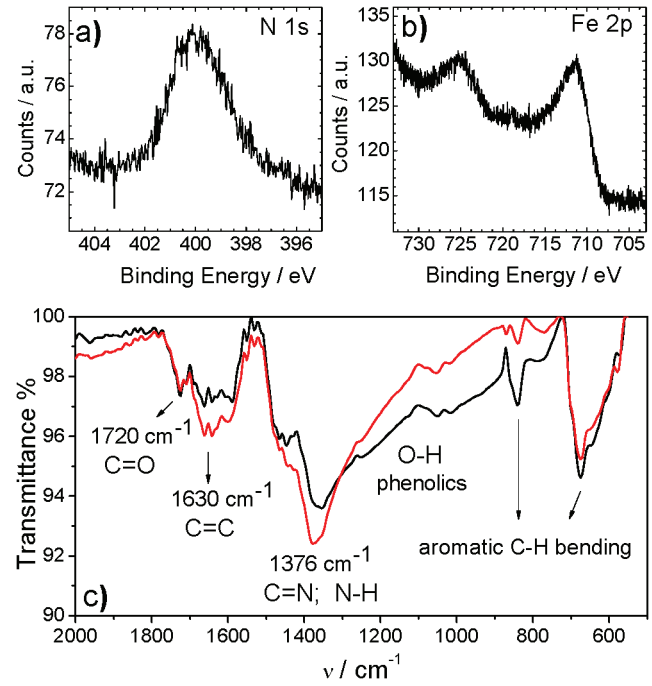

Figure 1. XPS data for iron−melanin ($t = 4$ h). (a) N 1s, (b) Fe 2p. (c) FTIR spectra of iron−melanin deposits supported on HOPG; $t = 4$ (black) and 14 h (red)

Results and Discussion

Characterization of the Iron−Eumelanin Deposits on HOPG. Figure 1a−b shows XPS data for iron−melanin deposits on HOPG ($t = 4$ h). The N 1s signal at 400 eV (Figure 1a), typical of melanin,[15] and Fe 2p at 710 eV (Figure 1b), typical of oxidized iron[7] are observed.

The IR spectra (Figure 1c) obtained from our system for $t =$ 4 and 8 h exhibit the signals corresponding to the melanins,[16] namely the characteristic quinone C═O stretching vibration at 1720 cm^{-1}, and a broadband around 1630 cm^{-1} related to C═C stretching vibration of aromatic units of the indole residues in the polymer. The strong and broadband around 1376 cm^{-1} involves contributions from aromatic C═N stretching and N−H bending modes[17,18] while bands ranging from 1000 to 1240 cm^{-1} should be assigned to C−O stretching vibration of alcoholic (phenolic) moieties.[18] The intensity of the melanin bands increases with the deposition time, i.e., as more melanin deposited on the HOPG surface. On the other hand, the low-frequency signals can be assigned to the C−H deformation of the aromatic rings and the C−O deformation of the phenol moieties. Contributions of oxidized iron species appear at frequencies smaller than 600 cm^{-1} (not shown).[19−22] It should be noted that similar spectra are recorded for the iron−melanin films grown on Au(111) and also in melanin powders.

The AFM image of the HOPG surface after depositing iron−melanin for $t = 4$ h shows ramified structures formed by granules with sizes ranging from 5 to 35 nm (Figure 2a). The electrochemical growth of melanin deposits on HOPG consists in the formation of a granular deposit that gradually covers the HOPG surface.[7] The deposition process starts at steps of the HOPG basal plane with the formation of small particles that reach sizes around 10 and 0.35−1 nm in height in 2 h. For $t >$ 2 h these particles begin to aggregate forming big ramified islands which finally overlap. After a 24 h polarization the film covers almost the entire surface, reaching heights in the order 3−10 nm. It is interesting to notice that even for the biggest aggregates it is always possible to distinguish small particles

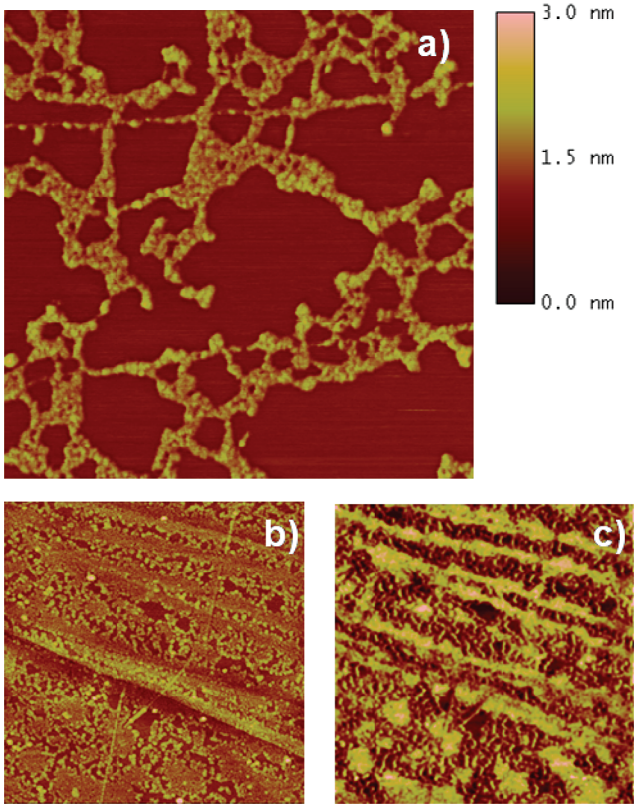

Figure 2. (a) 500 × 500 nm^2 AFM phase contrast image of the melanin deposit (t = 4 h) showing the formation of a granular structure. (b−c) 2500 × 2500 nm^2 MFM images of the melanin deposit (t = 8 h): (b) topographic image; (c) magnetic phase contrast image (lift mode). Different magnetized regions are visible through the relative size and intensity

as building blocks, whose sizes increase slightly with the electrodeposition time. This structure is particularly well detected using AFM imaging under the contrast phase mode (Figure 2a). Stabilization of the melanin deposits on the HOPG terraces could arise from $\pi-\pi$ interactions as the melanin granules exhibit a graphitic-like structure as suggested by the granule and island height (0.35−1.0 nm). Contributions from electrostatic interactions and hydrogen bonding can also play a key role at HOPG step edges, where different types of functional groups are present, explaining the preferential nucleation at these defects.

The magnetic contrast phase image (Figure 2b−c) shows very different iron-containing zones on the surface. Most of the iron-rich eumelanin deposits appear exactly following the HOPG steps, giving a strong magnetic contrast phase along those steps. In addition, on the terraces between steps (lower left corner) some isolated iron rich zones can be also detected with a strong magnetic phase contrast as well and randomly distributed. Finally, the rest of the surface shows a very weak phase contrast or even an almost no phase contrast at all. This magnetic behavior observed in the iron−melanin films grown on HOPG and on Au(111)[8] is in good agreement with previously reported magnetic character of the synthetic iron−melanins.[23]

The electrochemical response of iron−melanin deposits of different thickness (t = 4 and 8 h) in degassed TRIS pH 7.4 and in 0.1 M NaOH solutions is shown in Figure 3a−b. The melanin modified HOPG surface is electrochemically active in a wide potential range. As already reported the broad redox couple at −0.15/−0.30 V (AI′/CI′) shown in Figure 3a is assigned to the quinol/quinone redox couple present in the biopolymer while the broad peaks −0.6/−0.8 V (AI,CI,CII,CIII)

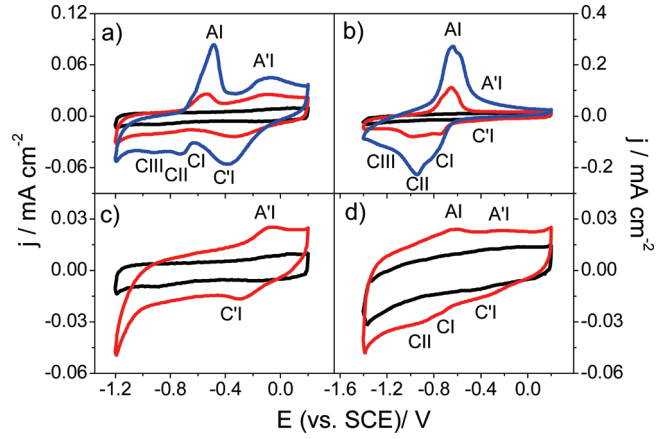

Figure 3. Stabilized voltammograms for iron−melanins covered HOPG; black, t = 0; clean HOPG: red, t = 4 h; blue, t = 8 h. (a) TRIS buffer pH 7.4, (b) 0.1 M NaOH. Stabilized voltammograms for HOPG (black) and QH/Q covered HOPG (red). (c) TRIS buffer pH 7.4, (d) 0.1 M NaOH. Scan rate 0.2 V s^{-1}.

can be assigned to Fe(III)/Fe(II) species coordinated to the melanin protomolecules.[7,8] It was proposed that four indol units coordinate single Fe ion.[24] As expected in alkaline medium the quinol/quinone redox couple (AI′/CI′) moves in the negative direction defining two waves at −0.3/−0.4 and −0.6/−0.8 V[25] that overlap in some extent to the Fe(II)/Fe(III) redox couples (AI/CI,CII,CIII) (Figure 3b).[7] The intensity of the voltammetric peaks and the charge involved increases markedly with the deposition time indicating an increase in the iron−melanin surface coverage, in agreement with the IR data.

The assignation of the AI′/CI′ voltammetric waves of the iron−melanin deposits to the quinone/quinol redox couples was confirmed by the voltammograms recorded for Q/QH supported on HOPG in degassed TRIS buffer pH 7.4 (Figure 3c) and 0.1 M NaOH (Figure 3d). In fact, the Q/HQ originates the AI′/CI′ redox couples in both neutral and alkaline solutions and also contributes in the potential range of AI/CI,CII in alkaline media.

Characterization of the Fe Sites in the Eumelanin. Concerning to the nature of Fe sites in eumelanin we perform XAFS characterizations on that sample and Fe-oxide reference compounds in order to determine the concentration of Fe(II)/Fe(III) ions and their local environment (symmetry, coordination, atomic distances, and density of Fe ions) in our synthetic eumelanin. A detailed discussion on these techniques, experimental results, and data analysis is presented in the Supporting Information. Here, we present a brief summary of our XAFS results that are important to understand the catalytic effect of the Fe species present in the eumelanin deposit.

According to the XANES results, sensible to electronic and symmetry characteristic of Fe absorbent atoms, the energy shift of the Fe K-edge in the corresponding sample spectra indicates a Fe^{3+}/Fe^{2+} ratio of about 9:1 being octahedral the symmetry of these sites (see Supporting Information, Figure S1a and b). EXAFS allow us the analysis of the local environment of Fe ions. The spectrum can be described by only one type of Fe site (central atom) in a structurally distorted arrangement close to Fe in Fe_2O_3 with a well-defined bond length, i.e., with three pairs of oxygen atoms as first neighbors (see Table 1). In a previous work Kropf and co-workers[24] assign two pairs of those oxygen atoms (O_1 in Table 1) as forming part of two quinone-like structures having (as in present case) a first-shell coordination number of about six (oxygen atoms). These authors suggest that the remaining pair of oxygen atoms (O_2, in Table 1) can be attributed to the hydration of the sample, out of the plane

TABLE 1: Fitted EXAFS Parameters (See *Supporting Information* for Experimental and Fitting Details) for First Oxygen Coordination Shell of Fe Present in the Eumelanin Sample[a]

coordination shell	average coordination number (*N*)	radial distance (Å)	Debye−Waller factor (Å^{-2})
O_1 (quinone units)	4.2(1)	2.00(5)	0.008(1)
O_2 (H_2O)	1.6(3)	2.18(5)	0.008(1)
Fe_1	0.6(5)	2.81(5)	0.004(3)
Fe_2	0.5(5)	2.95(5)	0.004(3)
Fe_3	0.3(5)	3.24(5)	0.004(3)

[a] Fe_i represents the different contributions to the total Fe−Fe first coordination shell. The total average coordination number N for Fe−Fe is obtained by the sum of the three Fe_i contributions: $Fe_1 + Fe_2 + Fe_3 = 0.6 + 0.5 + 0.3 = 1.4$. The Debye−Waller factor represents the thermal and structural disorder for the corresponding bonds to each coordination shell. Errors in last digit appear between brackets.

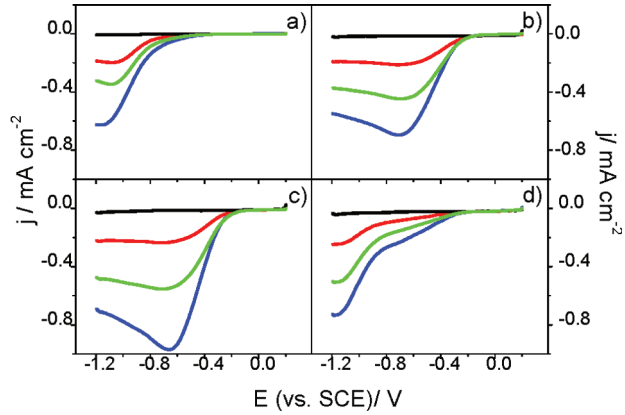

Figure 4. Voltammograms recorded at 0.2 V s^{-1} in TRIS buffer, pH 7.4, at different oxygen concentrations: 0 M (black), 2.75×10^{-4} M (red), 7×10^{-4} M (green), and 1.2×10^{-3} M (blue). (a) Clean HOPG, (b) iron−melanin on HOPG ($t = 4$ h), (c) iron−melanin on HOPG ($t = 8$ h), (d) QH/Q on HOPG.

determined by the two quinone-like structures. In the present case the corresponding Fe−O bond of 2.18 Å for oxygen from hydration results 0.18 Å larger than the four oxygen atoms bonded to Fe from the quinone structures (Table 1). Finally, according to EXAFS fitted parameters for Fe−Fe coordination shells, Fe centers appear nearly coordinated with three types of iron atoms (Fe_1, Fe_2, and Fe_3 in Table 1) at distances between 2.8 and 3.2 Å. According to the Fe−Fe total average coordination number in the sample (corresponding to the sum of the individual Fe_i contributions of each average Fe−Fe coordination number N, i.e., $0.9 + 0.3 + 0.2 = 1.4$), the melanin clusters appear coordinated with more than one Fe ion in average (i.e., forming dimers or trimmers of Fe units), which clearly differs from the Fe coordination of 6 as in the bulk Fe-oxide structure (see Figure 2S in Supporting Information).

Oxygen Electroreduction on HOPG and Modified HOPG Surfaces. In Figure 4a−c the voltammetric responses of clean HOPG and iron−melanin-covered HOPG surfaces in TRIS buffer (pH 7.4) at different oxygen concentrations are shown.

The oxygen electroreduction reaction (OER) on the clean HOPG surface in the TRIS buffer shows only a reduction wave at very negative potential values, $E < -1.1$ V, The current density associated to this wave increases with the oxygen concentration (Figure 4a). This wave can be assigned to the first electron step of the OER leading to hydrogen peroxide formation. The low reactivity of the graphite basal plane, which

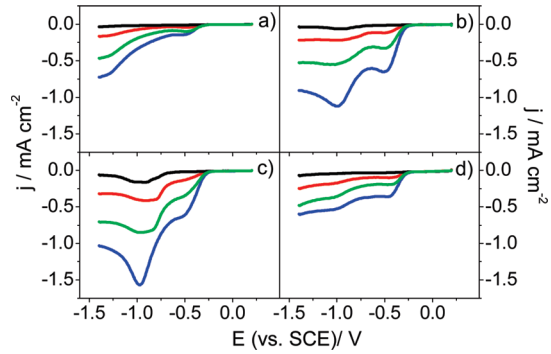

Figure 5. Voltammograms recorded at 0.2 V s^{-1} in 0.1 M NaOH at different oxygen concentrations: 0 M (black), 2.75×10^{-4} M (red), 7×10^{-4} M (green), and 1.2×10^{-3} M (blue). (a) Clean HOPG, (b) iron−melanin on HOPG ($t = 4$ h), (c) iron−melanin on HOPG ($t = 8$ h), and (d) QH/Q on HOPG.

requires high overpotentials, is a result of its low density of electronic states and the lack of functional groups and adsorption sites.[26,27] The basal plane of HOPG is unusual in that all the valencies are satisfied in the plane of surface.[28,29] In contrast, the OER on the iron−melanin-modified HOPG surface ($t = 4$ h) shows a well-defined wave at −0.65 V that also depends on the oxygen concentration (Figure 4b). As can be seen, the OER is positively shifted ≈0.45 V on the iron−melanin-covered surfaces in relation to the clean HOPG surface. Figure 4c also shows that thicker iron−melanin deposits ($t = 8$ h) produce a similar potential shift than thinner deposits. However, the electroreduction currents becomes larger than those recorded on the thinner iron−melanin deposits ($t = 4$ h). These results mean that increasing the surface coverage and thicknesses by iron−melanin results in larger electroreduction currents due to the increase in the number of active sites.

The results for the iron−melanin-modified surfaces are compared to those obtained for the Q/HQ-modified HOPG surfaces prepared with an amount of material comparable to that of the Fe−melanin system of $t = 8$ h (Figure 4d). In this case two waves in the oxygen-containing TRIS buffer are observed. The first one, poorly defined, appeared at −0.6/−0.7 V and can be assigned to the catalytic activity of the HQ/Q redox couple. In fact, it is well known that surface quinone groups are efficient electrocatalysts for OER.[30] The second one at −1.1 V can be associated to uncovered HOPG domains on the basis of the results shown in Figure 4a.

Some interesting conclusions can be drawn from the results shown in Figure 4. The first one is that the iron−melanin system exhibits a high OER catalysis in a potential range where the clean HOPG surface is inactive. This catalytic activity can be related to the quinol/quinone redox system present in the biopolymer as it is observed in the same potential range where the Q/HQ redox couple is active on HOPG. On the other hand, the HOPG surface modification is easier for the iron−melanin than for HQ/Q because it results in a larger number of active sites leading to well-defined electroreduction waves and higher currents.

The voltammograms recorded in 0.1 M NaOH are shown in Figure 5. First, the HOPG substrate exhibits a small prewave around −0.5 V (Figure 5a) that can be assigned to the catalytic activity of a small amount of active surface groups present on the carbon surface.[31,32] In particular, surface functionalities at plane defects of graphite are known to significantly increase O_2 reduction activity by acting as adsorption sites for oxygen and other intermediates. As already reported this prewave is

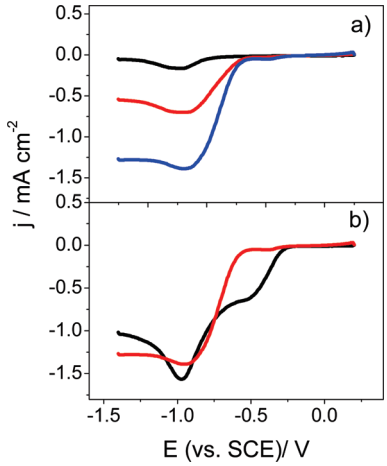

Figure 6. (a) Voltammograms recorded for iron−melanin covered HOPG (t = 8 h) on HOPG at 0.2 V s^{-1} in degassed 0.1 M NaOH at different hydrogen peroxyde concentrations: blank (black), 4 mM (red), and 12 mM (blue). (b) Voltammograms recorded for iron−melanin covered HOPG (t = 8 h) at 0.2 V s^{-1}: 12 mM hydrogen peroxide in degassed 0.1 M NaOH (red). Oxygen saturated 0.1 M NaOH (black).

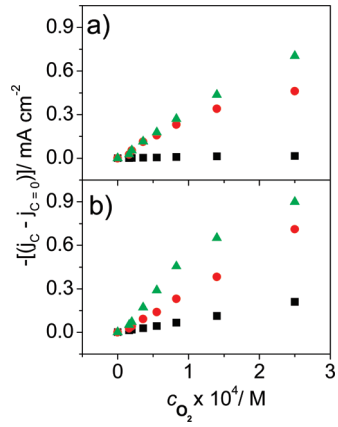

Figure 7. Stationary current density $j_c - j_{(c=0)}$ versus O_2 concentration plot for free HOPG (black square), t = 4 (red circle) and 8 h (green triangle) iron−melanin covered HOPG. j_c is the stationary current density read for the sample at −0.5 V for pH 7.4 (a) and at −0.9 V for pH 12.6 (b), and $j_{(c=0)}$ is the current density read for a O_2-free solution at the same potential.

only evident for pH values greater than 10.[25] However, net currents related to OER are observed only in a poorly defined wave at $E < -1.2$ V.

On the other hand, for the iron−melanin-covered HOPG we observe two well-defined waves at −0.5 and −0.9 V (Figure 5b−c). In principle the second wave can be assigned to the hydrogen peroxide electroreduction. In fact, in Figure 6a the voltammograms recorded for iron−melanin-covered HOPG in degassed 0.1 M NaOH solution containing different amounts of hydrogen peroxide are shown. The hydrogen peroxide electroreduction originates well-defined waves at −0.9 V with a concentration-dependent current density.

In Figure 6b we compare voltammograms recorded in oxygen saturated solution and that recorded in 12 mM hydrogen peroxide. From these results we can conclude that the second wave at −0.9 V recorded in the oxygen-containing solutions is due to the hydrogen peroxide electroreduction. Note also the enhanced electrocatalysis for oxygen and hydrogen peroxide electroreduction of the iron−melanin system in relation to the clean HOPG surface.

Voltammograms recorded for HQ/Q deposits on HOPG (similar amount of deposited charge to the iron−melanin deposit of t = 8 h) exhibit the first reduction wave related to the oxygen electroreduction to peroxides in the same potential range than that observed for the iron melanin modified HOPG, although the associated currents are smaller (Figure 5d). Besides, the second wave at −0.9 V is also too small in relation to the first one indicating that the contribution of the hydrogen peroxide electroreduction to hydroxyl species is not significant on the Q/HQ modified HOPG, in agreement with previous observations.[25]

Figure 7a−b summarizes OER results by plotting the stationary current density $j_c - j_{(c=0)}$ versus O_2 concentration plot for clean HOPG and iron−melanin-covered HOPG in TRIS buffer (Figure 7a) and 0.1 M NaOH (Figure 7b) solutions. These plots demonstrate the linear correlation between the measured currents and the oxygen concentration, as well as the strong influence of iron melanin on modifying the surface chemistry of the HOPG substrate increasing the catalytic activity.

Finally, the open circuit potential (ocp) of the iron−melanin-covered HOPG (t = 8 h) was measured in the oxygen saturated TRIS buffer. After immersion the ocp rapidly reaches a stable value around −0.05 V, that is the potential region of the Q/HQ redox couple observed in Figure 3c. The increase in pH to 13 results in a decrease in the ocp that stabilizes at −0.15 V. The 0.02 V/pH unit is consistent with previous observations for the pH dependence of iron(II) phthalocyanines.[33] The nitrogen bubbling (to remove oxygen) in the solution or the increase in pH also result in an ocp shift toward more negative values. Therefore, the spontaneous potential that the iron−melanin modified HOPG reaches in neutral media is controlled by the quinol/quinone species, O_2, and pH.

Now we discuss the processes taking place during oxygen reduction on the iron−melanin-covered HOPG. We propose that the first wave in the electroreduction curve is related to O_2 reduction to peroxide species mediated by the quinol/quinone groups present in the iron−melanin films (see Figure 1c). In the −0.2/−0.4 V potential range, where the electrocatalytic process for O_2 starts to be observed (Figure 4−5), semiquinone radicals are produced as the quinone species are reduced to quinol (Figure 3). In fact, it is believed that the oxygen reduction rate is proportional to the surface concentration of the semiquinone radical formed by the electrochemical reduction of quinone groups.[32] The radical anion $O_2^{\bullet -}$ reacts with molecular oxygen to yield the superoxide anion, O_2^-, which either disproportionates or follows an electrochemical−chemical mechanism.[32] The reactions catalyzed by the quinone/quinol redox couple of the iron−melanin granules can be written as follows

$$O_2 + e \rightarrow O_2^{\bullet -} \quad (1a)$$

$$O_2^{\bullet -} + H_2O + e \rightarrow HO_2^- + OH^- \quad (1b)$$

Note that the participation of iron species in this reaction is unlikely in the potential windows of the quinol/quinone redox couple. In fact, in the −0.2/−0.4 V range the iron atom, which is coordinated with the two pairs of oxygen atoms that form part of two quinone-like structures (see Supporting Information and ref 21), should be in the Fe(III) oxidation state as it occurs for the iron atoms in our synthetic eumelanin exposed to ambient conditions (Fe(IIII)/Fe(II) ratio ≈ 9). It is well known that Fe(III) is not favored as active site for O_2 reduction because H_2O bonds

strongly to this site as we observe in the synthetic eumelanin (hydration molecules, Table 1), blocking it against O_2 adsorption.[34] In contrast, Fe(II) is predicted to be the active site for the four-electron reduction of oxygen by iron macrocycles.[35,36] The Fe(II) species become predominant at potentials more negative than $-0.6/-0.7$ V. Thus, in this potential range O_2 molecules can bind the Fe(II) sites to form (OHOH) species.[34] The O lone-pair donation bond to the Fe(II) center is proposed to prevent hydrogen peroxide from leaving as a two-electron reduction product providing a path for reduction to water. Also $O_2^{\bullet -}$ species can reduce Fe(III) to Fe(II) species[37] according to

$$O_2^{\bullet -} + \text{Fe(III)} = \text{Fe(II)} + O_2 \qquad (1c)$$

The presence of Fe(II) in the biopolymer explains the second wave clearly observed in alkaline solutions. In this case the reactions leading to radical formation catalyzed by the Fe(II)−quinone/quinol redox couples of the iron melanin granules can be written

$$O_2 + 2H_2O + 4e \rightarrow 2HO^{\bullet} + 2OH^- \qquad (2a)$$

$$H_2O_2 + 2e \rightarrow HO^{\bullet} + OH^- \qquad (2b)$$

In neutral media only one oxygen reduction wave is observed suggesting either a direct four-electron reduction (reaction 2a) or a partial overlap of the potential range where reaction 1 and 2b take place.

This interpretation accounts for the key role of iron−melanin system in lipid peroxidation. In fact, the strong ability of eumelanins to produce reactive oxygen species arises from a synergistic action of the quinone/quinol and Fe/quinone/quinol redox couples that allow oxygen reduction in a wide potential range. The quinone/quinol pathway leads to the formation of peroxide species that then can enter into the Fe/quinone/quinol system yielding the highly aggressive hydroxyl species. This species resulting from reaction 2 lead to lipid (LH) peroxidation according to

$$LH + HO^{\bullet} = L^{\bullet} + H_2O \qquad (3)$$

In contrast to $HO^{\bullet}$, the $O_2^{\bullet -}$ radical resulting from reaction 1a is too weak oxidant to initiate reaction 3.[3] Increased levels of iron have been observed in dopaminergic neurons in Parkinson disease.[38] Iron levels in the order of 3.3 mg/g were determined in purified neuromelanin.[39] The iron-chelating feature of some quinones in conjunction with their moderate hydrophylicity are the more important requisites for lipid peroxidation.[40] The iron-rich regions of the granular melanin deposit (Figure 2) can be responsible for the production of hydroxyl species.

It has been reported that eumelanins are unable to reduce O_2 by themselves.[41] In fact, the electrochemical potential of neuromelanin granules and melanosomes is -0.35 ± 0.2 V vs SCE that is not sufficiently reductive to generate a high level of oxidative stress.[39] It has not been possible to assign the electrochemical potential to a specific chemical species on the surface because the molecular structure of these pigments remains elusive, and also they contain lipids, proteins, and metallic cations.[41] However, it has also been observed that this potential is independent of Fe(III) concentration.[42] We note that the -0.350 ± 0.2 V potential value is not far to the potential range of the quinone/quinol redox couple observed in our electrochemical experiments. We suggest that the electrochemical potential of eumelanins is determined by these functional groups.

Conclusions and Outlooks

Our results show that iron-containing eumelanin granules are efficient catalysts to reduce oxygen to water, thus producing reactive oxygen species along the reaction. Therefore, the iron-rich melanin granules should be able to couple oxygen reduction with lipid oxidation. The quinone/quinol groups in melanins determine the open circuit potential suggesting that they also determine the electrochemical potential observed in eumelanin granules and melanosomes. The quinone/quinol groups are also responsible of the $O_2^{\bullet -}$ production. The key role of Fe(II) species to catalyze the complete oxygen reduction to water producing aggressive $HO^{\bullet}$ radical is also stressed. Our electrochemical study provides new evidence for a better understanding the neurotoxic effect of the iron melanin system.

Finally, from the point of view of electrocatalysis it should be interesting to explore the ability for oxygen reduction of melanin-like films prepared by different strategies such as those described in refs 11 and 12.

Acknowledgment. We acknowledge financial support from ANPCyT (PICT 06-621, PICT 08-38) and CONICET (PIP112-200801-03079, PIP 112-200801-00362) (Argentina), and MCI (CTQ2008-06017/ BQU) (Spain). This paper was made in the frame of the Interfacial, Supramolecular and Molecular Nanoscience and Nanotechnology Net (PAE 22711, ANPCyT). R.C.S. is a Guggenheim Foundation Fellow. A.G.O. acknowledges MEC for a FPU fellowship.

Supporting Information Available: Detailed theoretical information and a complete discussion and interpretation about the data obtained by XANES and EXAFS techniques, including some specific references. This material is available free of charge via the Internet at http://pubs.acs.org.

References and Notes

(1) d'Ischia, M.; Napolitano, A.; Pezzella, A.; Meredith, P.; Sarna, T *Angew. Chem., Int. Ed* **2009**, *48*, 2–10. Meredith, P.; Riesz, J. *Photochem. Photobiol.* **2004**, *79*, 211.

(2) Liu, Y.; Kempf, V.; Samokhvalov, A.; Simon, J. D. *Pigment Cell Res* **2003**, *16*, 608. Szpoganicz, B.; Gidanian, S.; Kong, P.; Farmer, P *J. Inorg. Biochem.* **2002**, *89*, 45.

(3) *Neurotoxic Factors in Parkinson's Disease and Related Disorders*; Storch, A.; Collins, M. A., Eds.; Springer: New York, 2001. Ben-Shachar, D; Youdim, M. B. *Prog. Neuropsychopharmacol. Biol. Psych.* **1993**, *17*, 139–50. Zecca, L.; Zucca, F. A.; Wilms, H; Sulzer, D *Trends Neurosci.* **2003**, *26*, 578–580.

(4) Kimura, S.; Kurasaki, M.; Saito, T.; Ito, K.; Hosokawa, T.; Okabe, M.; Shiraishi, K.; Niioka, T *Neurosci. Res. Commun.* **2001**, *29*, 31–40.

(5) Hong, L.; Liu, Y.; Simon, J. D. *Photochem. Photobiol.* **2004**, *80*, 477–481. HallE. D., Andrus, P. K. Current Protocols in Neuroscience 2001, DOI: 10.1002/0471142301.ns0717s11.

(6) Díaz, P.; Gimeno, Y.; Carro, P.; González, S.; Schilardi, P. L.; Benítez, G.; Salvarezza, R. C.; Hernández Creus, A. *Langmuir* **2005**, *21*, 5924–5930.

(7) González Orive, A.; Gimeno, Y.; Hernández Creus, A.; Grumelli, D.; Vericat, C.; Benitez, G.; Salvarezza, R. C. *Electrochim. Acta* **2009**, *54*, 1589–1596.

(8) Orive, A.; Dip, P.; Gimeno, Y.; Diaz, P.; Carro, P.; Hernandez Creus, A.; Benitez, G.; Schilardi, P. L.; Andrini, L.; Requejo, F.; Salvarezza, R. C. *Chem.−Eur. J.* **2007**, *13*, 473.

(9) Hegedus, J. L. *Toxicology* **2000**, *145*, 85–101.

(10) DuVall, S. H.; McCreery, R. L. *J. Am. Chem. Soc.* **2000**, *122*, 6759–6764.

(11) Lee, H.; Dellatore, S. M.; Miller, W. M.; Messersmith, P. B. *Science* **2007**, *318*, 426–430.

(12) Bernsmann, F.; Ponche, A.; Ringwald, C.; Hemmerlé, J.; Raya, J.; Bechinger, B.; Voegel, J. C.; Schaaf, P.; Ball, V. *J. Phys. Chem. C* **2009**, *113*, 8234–8242.

(13) Cataldo, F. *Polym. Int.* **1998**, *46*, 263–268.

(14) (a) Kruusenberg, I.; AlexeyevaN., Tammeveski, K. Carbon 2009, 651−658; and(b) Jürmann, G.; Tammeveski, K. *J. Electroanal. Chem.* **2006**, *597*, 119–126.

(15) Clark, M. B.; Gardella Jr, J. A.; Schultz, J. M.; Patil, D. G.; Salvati, L, Jr. *Anal. Chem.* **1990**, *62*, 949.

(16) Centeno, S. A.; Shamir, J *J. Mol. Struct.* **2008**, *873*, 149–159.

(17) Capozzi, V.; Perna, G; Gallone, A; Biagi, P. F.; Carmone, P; Fratello, A; Guida, G; Zanna, P; Cicero, R *J. Mol. Struct.* **2005**, *744−747*, 717–721.

(18) Samokhvalov, A.; Liu, Yan; Simon, J. D. *Photochem. Photobiol.* **2004**, *80*, 84–88.

(19) Bilinska, B. *Spectroquim. Acta Part A* **1996**, *52*, 1157–1162.

(20) Cheng, C. M; Kou, G; Wang, X. L; Wang, S. H; Gu, H. C; Guo, Y. J *J. Magn. Magn. Matter.* **2009**, *321*, 2663–2669.

(21) Bautista, M. C; Bomati-Miguel, O; Morales, M. P; Serna, C. J; Veintemillas-Verdaguer, S *J. Magn. Magn. Matter.* **2005**, *293*, 20–27.

(22) Prasad, P. S. R; Shiva Prasad, K; Krishna, C.; Babu, E. V. S. S. K; Sreedhar, B; Ramana, M. S *J. Asian Earth Sci.* **2006**, *27*, 503–511.

(23) Bolzoni, F.; Giraudo, S.; Lopiano, L.; Bergamasco, B.; Fasano, M.; Crippa, P. R. *Biochim. Biophys. Acta* **2002**, *1586*, 210–218.

(24) Kropf, A. J.; Bunker, B. A.; Eisner, M.; Moss, S. C.; Zecca, L.; Stroppolo, A.; Crippa, P. R. *Biophys. J.* **1998**, *75*, 3135.

(25) Jürmann, G.; Schiffrin, D. J.; Tammeveski, K *Electrochim. Acta* **2007**, *53* (1), 390–399.

(26) Cline, K,; McDermott, M. T.; McCreery, R. L. *J. Phys. Chem.* **1994**, *98*, 5314.

(27) McIntyre, R.; Scherson, D.; Storek, W.; Gerischer, H. *Electrochim. Acta* **1987**, *32*, 51.

(28) Randin, J. P.; Yeager, E. *J. Electroanal. Chem.* **1972**, *36*, 257.

(29) Randin, J. P.; Yeager, E *J. Electrochem. Soc.* **1971**, *118*, 711.

(30) Nagaoka, T.; Sakai, T.; Ogura, K.; Yoshino, T. *Anal. Chem.* **1986**, *58*, 1953.

(31) Hossain, M. S.; Tryk, D.; Yeager, E. *Electrochim. Acta* **1989**, *34*, 1733.

(32) Tammeveski, K.; Kontturi, K.; Nichols, R. J.; Potter, R. J.; Schiffrin, D. J. *J. Electroanal. Chem.* **2001**, *515*, 101.

(33) Zhao, F.; Harnisch, F.; Schro, U; Scholz, F.; Bogdanoff, P.; Herrmann, I. *Electrochem. Commun.* **2005**, *7*, 1405–1410.

(34) Anderson, A. B.; Sidik, R. A. *J. Phys. Chem. B* **2004**, *108*, 5031–5035.

(35) Kobayashi, N.; Nishiyama, Y. *J. Phys. Chem.* **1985**, *89*, 1167.

(36) Khorasani-Motlagh, K, M.; Noroozifar, M.; Ghaemi, A.; Safari, N. *J. Electroanal. Chem.* **2004**, *565*, 115.

(37) Benov, L. *Protoplasma* **2001**, *217*, 1–3.

(38) Oakley, A E; Collingwood, J F; Dobson, J; Love, G; Perrott, H R; Edwardson, J A; Elstner, M; Morris, C M *Neurology* **2007**, *68*, 1820–5.

(39) Depboylu, C.; Matusch, A.; Tribl, F.; Zoriy, M.; Michel, P. P.; Riederer, P.; Gerlach, M.; Becker, S.; Oertel, W. H.; Höglinger, G. U. *Neurodegenerative Dis.* **2007**, *4*, 2–3.

(40) Alegría, A. E.; Santiago, G. *Toxicol. Environ. Chem.* **1998**, *65*, 185–202.

(41) Bush, W. D.; Garguilo, J.; Zucca, F. A.; Albertini, A.; Zecca, L.; Edwards, G. S.; Nemanich, R. J.; Simon, J. D. *Proc. Natl. Acad. Sci. U.S.A.* **2006**, *103*, 14785–14789.

(42) Simon, J. D. *Pigment Cell Res.* **2006**, *19*, 527–528.

JP905560D